IEEE Access
Multidisciplinary ⋮ Rapid Review ⋮ Open Access Journal

Received 26 May 2024, accepted 14 June 2024, date of publication 19 June 2024, date of current version 28 June 2024.

Digital Object Identifier 10.1109/ACCESS.2024.3416466

RESEARCH ARTICLE

Research on the Design of Mechanically Sealed Switch Based on Permanent Magnet Eddy Current Transmission Characteristic

WANG TENG[1,2,3,4], WU YIPENG[1,3], SONG TAO[1,2,3,4], AND GUO WENXIAO[1,2,3,4]

[1]CCTEG Taiyuan Research Institute Co., Ltd., Taiyuan 030006, China
[2]Shanxi Tiandi Coal Mining Machinery Co., Ltd., Taiyuan 030006, China
[3]China Coal Research Institute, Beijing 100013, China
[4]China National Engineering Laboratory for Coal Mining Machinery, Taiyuan 030006, China

Corresponding author: Wang Teng (wangteng40@126.com)

This work was supported in part by the Chinese National Key Research and Development Program under Grant 2022YFB4703604, in part by Shanxi Provincial Patent Transformation under Project 202305002, in part by the Intelligent Roadway Trenching Robot Application on Confined Mining Area and the Scientific Research Projects of Shanxi Tiandi Coal Machinery Company Ltd. under Grant M2021-MS08, in part by the Special Project of Science and Technology Innovation Venture Capital of Tiandi Technology Company Ltd. under Grant 2023-TD-ZD013-001 and Grant 2023-TD-ZD004-002, in part by Shanxi Province Key Research and Development Project under Grant 202202150401018, and in part by Shanxi Tiandi Coal Machinery Equipment Company Ltd. under Grant M2023-ZD09.

ABSTRACT Aiming at the difficulty in designing the internal spray system inside the telescopic cut-off head of coal mine machinery, this study proposes a mechanical seal switching principle based on the permanent magnetic eddy current effect, which realizes the switching and sealing between the cylinder's expansion state (without rotation) and the internal spray condition (with rotation). This work can solve the current problem that the inner spray cannot be arranged inside the external rotor structure mining equipment. Firstly, the mechanical seals of the two working conditions are designed, and the requirements for the torque and axial force of the permanent magnet eddy current structure are proposed, and the sealing conditions and mutual switching conditions of the cylinder working condition and spray working condition are revealed. Secondly, the mathematical description of the eddy current magnetic field of the permanent magnet eddy current valve is established, and the calculation equations of the torque and axial force of the permanent magnet eddy current transmission are proposed, and a calculate study is carried out by using the finite element method, and the calculation results show that in the low-slip region, the analysis of the electromagnetic torque and axial force characteristics of the permanent magnet eddy current and the finite element results are in good agreement. Finally, example simulations show that the permanent magnet eddy current switch can realize the sealing and its switching between the two operating conditions as desired, and can realize the low leakage operation.

INDEX TERMS Mechanical seal design, permanent magnet eddy current drive, internal spray, extractive machinery.

I. INTRODUCTION

All underground extractive mining machines have a cutting head, which is used to cut coal, such as the cutting drum of coal mining machine and the cutting head of road-header. The cutting head will generate dust and sparks when cutting coal, consequently, equipping the cutting head with external and internal spray systems is vital to facilitate the cooling of the cutting teeth, eliminate the sparks of the cutting teeth, and thus reduce the dust concentration in the working face. Usually, the cutting head is an external rotor structure, the shaft is fixed, the shell rotates, the working speed is usually below 50 rpm, and the working pressure of the internal spray is 3∼4 MPa. The internal spray system is generally arranged in the connection between the cutting drum and the cantilever arm, and it enters into the internal part of

The associate editor coordinating the review of this manuscript and approving it for publication was Guido Lombardi.

the rotating cutting drum after the shaft is fixed, and sprays outward through the nozzles, so as to realize the function of cooling the cutting pick and spraying the dust reduction. However, there are some cutting drums that not only rotate, but also can be axially retracted, and the inlet and return ports of the retracting cylinder occupy the water inlet channel of the fixed shaft in the middle of the drum, which makes it difficult to realize the functions of cooling the cutting gears, spraying the dust and eliminating the sparks through the internal spray [1]. There is currently no design available that enables the spraying of variable-width cut-off drums with an internal spraying system from the cutting pick holder. Failure or non-functioning of the internal spray system may not only lead to premature failure of the cutting pick, affecting the mining progress of the working face, but may also lead to major safety accidents caused by sparking of the cutting pick.

In order to solve the design problem of the internal spray system of the retractable cutting drum of underground extractive mining machinery, the authors propose to use the oil supply line in the center of the cutting mechanism as the water supply line, and at the same time replace the retractable cylinder with a water medium cylinder, the water medium is used for the cylinder to retract and for spraying, and then put forward a kind of mechanically-sealed reversing switch based on the role of the permanent magnetic eddy current, when the cutting head cuts off the working condition (the cutting head rotates), the water medium is sprayed out from the cutting teeth of the cutting drum to realize the function of internal spraying; when the cutting head is in cutting condition (the cutting head is rotating), the water medium is sprayed out from the teeth of the cutting drum to realize the function of internal spraying, and when the cylinder is in telescopic condition (the cutting head is not rotating), the water medium enters into the cylinder to realize the telescopic action of the cutting drum. This design was adopted because water is currently used in mining machines to cool cut-off motors and cutting reducer, and this water, purified by filters and backwash units, can also be used to drive the cylinders and for spraying. The basic principle is to use the torque and axial force generated during the slip drive of permanent magnet eddy current mechanism to realize the switching of two kinds of working conditions. When the cutting head does not rotate (static), the attraction of the conductor disk yoke iron to the permanent magnet of the magnet disk completes the closure of the mechanical seal, and carries out the cylinder expansion and contraction action, while in the rotating of the cutting head, with the help of the mechanical mechanism, the pulling torque of the permanent magnet eddy current drive will be transformed into the axial force, and with the electromagnetic axial force, it realizes the switching of the cylinder condition to the spraying condition, and the switching valve will be reset again for the cylinder expansion and contraction working condition when the slip disappears. The design theory of permanent magnet eddy current switching valves involves both permanent magnet eddy current drive and mechanical sealing technologies.

The basic principle of permanent magnet eddy current flexible drive technology is to follow the basic law of magnetic induction, namely ''Lenz law''. When the conductor disk rotates, the slip of the conductor disk and the permanent magnet disk generates the cutting magnetic line of force movement, which generates the eddy current in the conductor disk, and the eddy current generates the inverse magnetic field around the conductor disk, which drives the permanent magnet disk to rotate, realizing the energy transfer in the air. Reference [2] examined the axial force characteristics between the permanent magnet eddy current coupler's conductor disc and magnet disc and came to the conclusion that these characteristics are similar to an exponential decay curve when the axial force and rotational speed difference are increased. Specifically, the magnet disc exhibits gravitational force between the conductor disc and the magnet disc when the two are relatively stationary, but as the rotational speed difference increases, the gravitational force decreases and becomes repulsive. The analysis of the axial force and rotative speed differential properties of permanent magnet eddy current transmission necessitates an examination of its electromagnetic field problem. Scholars have undertaken extensive research on the electromagnetic field problem when analyzing the torque characteristics of permanent magnet eddy current transmission. Currently, the main theoretical analysis methods for permanent magnet eddy current drives include the layer model [3], the equivalent magnetic circuit method [4], and the separated variable method (subdomain analysis method) [5], and the computational models used are the two-dimensional right-angle coordinate expansion model and the column coordinate model.

Reference [3] used layer model theory to reveal the torque-slip characteristics and axial force-slip characteristics of permanent magnet eddy current drives, whose torque characteristics are similar to the mechanical characteristics of asynchronous motors, while their axial force characteristics are first gravitational, and then gradually transformed into repulsive force with the increase of slip. Reference [6] studied in detail the axial force characteristics of disk-type permanent magnet eddy current drives, revealing the trend and mechanism of axial force characteristics change. Based on the equivalent surface current method, reference [7] deduced the computational expression for the axial force of the speed-regulated squirrel-cage asynchronous magnetic coupling for helical advance and retreat at low rotational speeds, and it was concluded that the axial force showed a tendency of increasing first and then decreasing from the fully engaged state to the disengaged state. Reference [8] and [9] combined with the equivalent magnetic circuit method and the magnetic circuit of the Kirchhoff's law to establish a solid disk permanent magnet coupler axial magnetization coupler model, the coupler's magnetic circuit parameters through analytical calculations of the model, and then combined with

the three-dimensional correction coefficients and torque formula to get the coupler's torque expression, the results of its results and the results of the finite element analysis with a better consistency. Reference [10] for permanent magnet eddy current couplers with slotted conductor disks investigated the analytical model of such couplers by the separated variable method and verified the accuracy of the model by finite element experiments. Reference [11] obtained a vector magnetic potential flux solution for the conductor region of a slotted conductor disk using the subdomain analytical method (separated variables method), and the results are consistent with those of the finite element analysis. Reference [12] established a layer model and vector magnetic potential expression considering alternately the conductor layer material, from which the magnetic field characteristics and torque expression of the slotted disk magnetic coupler were calculated. Their results show that the two-dimensional analytical modeling method and finite element results are in good agreement with the experimental results. Reference [13] also proposed a speed governing mechanism for a cylinder permanent magnet coupler with adjustable conductivity, and the torque characteristics of the cartridge permanent magnet eddy current governor were investigated using the separated variable method based on a two-dimensional expansion model. Reference [6] analyzed the electromagnetic field of a permanent magnet coupler in axial flux using the magnetic circuit method. However, there has not been any research on the use of disk-type permanent magnet eddy current coupler as a sealing compensation mechanism; the previous research can provide reference for the analysis of torque and axial force in this paper.

This paper firstly introduces the working principle of the permanent magnet eddy current switching valve for external rotor, designs the mechanical seals for two working conditions based on the mechanical seal design theory, and puts forward the axial force requirements that need to be provided for the permanent magnet drive, secondly, establishes the mathematical description of the eddy current magnetic field of the permanent magnet eddy current valve, puts forward the calculation equations of the torque and axial force of the permanent magnet eddy current drive, and cross-checks with the results of the finite element calculation analysis. Finally, through numerical simulation of the permanent magnet eddy current switching valve, the sealing state and leakage condition of the permanent magnet eddy current switching are investigated under different pressures.

II. PRINCIPLE OF OPERATION OF PERMANENT MAGNET EDDY CURRENT SWITCHING VALVE

The permanent magnet eddy current switching valve should have the following functions: firstly, the cylinder working condition, the cutting drum is static, the pressure water will be transported from the water supply shaft to the retractable cylinder, the internal cylinder of the cutting department can be retractable; secondly, the spraying condition, when the cutting drum rotates and cuts, the pressure water circuit will be switched to the internal spraying water circuit, and it will be reset to the cylinder working condition automatically when the cutting drum stops rotating. Therefore, the permanent magnet eddy current switching valve can reliably switch between the two working conditions. According to the above requirements, this paper designs the structure of permanent magnet eddy current switching valve, as shown in Fig. 1. According to the literature [14] and [15], for the acidic water in downhole, carbon graphite is selected for the dynamic ring material and silicon carbide is selected for the static ring material, and this pair of friction sub-combination can be applied to a variety of media such as water, oil and gas, and has good corrosion resistance.Stainless steel, which is not magnetically conductive, is used as the material of the parts except for the conductor disk assembly and the magnet disk assembly. This prevents the influence of other ferromagnetic parts as well as external electromagnetic fields on the permanent magnet coupling drive.

The water supply shaft 13 is stationary, and the shaft 13 is coupled with the magnet disk assembly (permanent magnet 3, frame 18, back iron 2 right cover 7) through the steel ball 14, constituting a force amplification mechanism for the torque to axial force; the frame 18 and the right translucent cover 7 are inlaid with a sealing ring; the left flange 1 and the right flange 6 are fixed together by bolts, and inside the right flange 6 there is inlaid a conductor disk 4, the end surface of which is parallel to the magnet disk, and between the conductor disk and the right flange is inlaid with a conductor

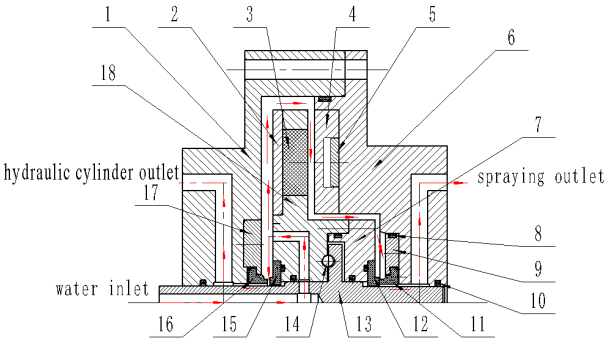

FIGURE 1. Structural schematic diagram of external rotor permanent magnet eddy current switching valve.

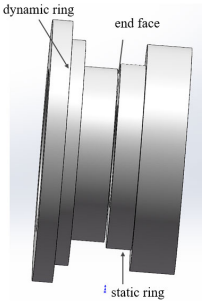

FIGURE 2. Mechanical seal structure schematic diagram.

TABLE 1. Units for magnetic properties.

No.	subassembly	NO.	subassembly
1	Left Flange	10	Glyd Ring
2	Magnet Disk Backing-iron	11	Right dynamic ring
3	Permanent Magnet Array	12	Right Static Ring
4	Copper Disk	13	Water Supply Shaft
5	Conductor Disk Yoke Iron	14	Steel Ball
6	Right Flange,	15	Left Static Ring
7	Right Cover Plate	16	Left Dynamic Ring
8	O-ring	17	Large Gland
9	Small Gland Plate	18	Magnet Disk Frame

disk yoke, the distance between which and the magnet disk is adjustable, which is used to adjust the electromagnetic gravitational force and torque between the conductor disk and the magnet disk. The left flange and right flange are inlaid with sealing rings 16 and 11, which form two mechanical seals with sealing rings 15 and 12 respectively.

The working principle of the device is as follows: in the cylinder condition, between the conductor disk assembly of the transmission device and the magnet disk assembly, there is only the suction force of the conductor disk yoke iron, and this suction force makes the medium pressure and the sealing closure force of the cylinder condition to reach equilibrium; in the spraying condition, the combined force between the conductor disk assembly of the transmission device and the magnet disk assembly consists of three parts: the suction force of the conductor disk yoke iron, the repulsive force of the eddy current field of the conductor disk copper disk, and the amplified axial repulsive force by the force booster mechanism. and the axial repulsive force amplified by the force multiplier mechanism. These combined forces cause the closing force of the cylinder condition seal to be overcome, thus opening that seal and pushing the left seal of the spray condition closed; in the event of a shutdown, there is only the suction force of the conductor disk yoke iron layer of the conductor disk assembly of the drive and the magnet disk assembly, and this suction force causes the closing force of the seal of the spray condition to be overcome, thus opening that seal and realizing the seal of the cylinder condition.

The performance requirements of permanent magnet eddy current switching valve is shown in Table 2.

TABLE 2. Performance requirements of permanent magnet eddy current switching valve.

Operational parameters	Values
Rotate speed	0~1500 rpm
Flow rate	40 L/min
Inlet pressure	≥3 MPa
Spraying outlet pressure	≥2.5 MPa
Cylinder outlet pressure	≥3 MPa
Leakage rate	3 ml/h
Mechanical seal face pressure	0.3~0.6 MPa

III. MECHANICAL SEAL DESIGN OF PERMANENT MAGNET EDDY CURRENT SWITCHING VALVE

Based on reference [14], the following assumptions are made when modeling the force analysis:

(1) The fluid flow between the mechanical seal end faces is laminar flow of incompressible viscous fluid.

(2) Seal end faces are parallel end faces, and the contact is regarded as the contact between the rough surfaces of the micro-convex body and randomly distributed on the contact surface.

(3) Neglecting the interaction between neighboring micro-convex bodies during the contact process, the friction between micro-convex bodies, the contact reinforcement effect and the change of hardness with depth.

(4) Changes in end load and frictional wear of the contacting end faces do not affect the distribution of micro-bumps.

(5) The change of fluid viscosity in the sealing gap and the rotation of the fluid are not considered.

A. SEAL DESIGN FORCE ANALYSIS

1) CYLINDER WORKING CONDITION FORCE ANALYSIS

Cylinder operating conditions, the magnet disk force is shown in Figure 3. The two ends of the magnet disk are subjected to hydraulic medium pressure, gravitational force of the magnet and the conductor disk yoke, repulsive force of the conductor copper disk on the magnet disk, axial thrust converted from the permanent magnet eddy current torque (if rotative speed difference exists), liquid film support on the sealing contact surface, and micro-convex body support force, respectively. The analytical calculation of each force is as follows:

The magnet disk is subjected to a combined pressure F_l of the fluid medium p_l inside the sealing end face:

$$F_l = \int_{D_a}^{D_m} p_l \cdot \frac{\pi}{2} d\mathrm{d}d - \int_{D_o}^{D_m} p_l \cdot \frac{\pi}{2} d\mathrm{d}d = \int_{D_a}^{D_o} p_l \cdot \frac{\pi}{2} d\mathrm{d}d \tag{1}$$

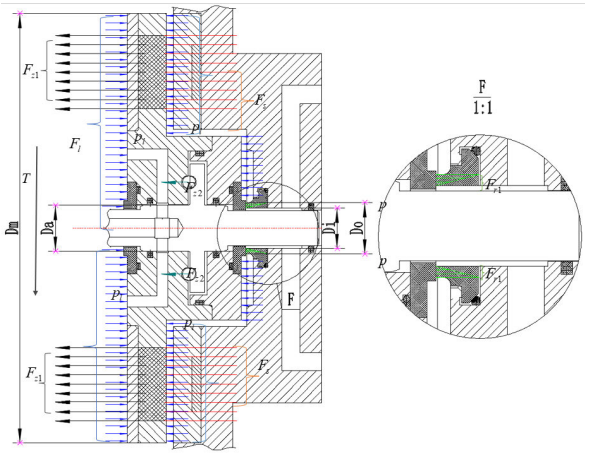

FIGURE 3. Cylinder working condition sealing force diagram.

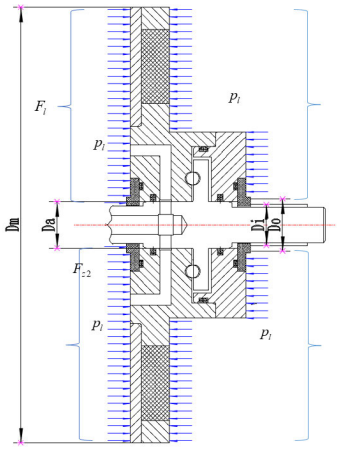

FIGURE 4. Fluid combined pressure.

where p_l for the medium pressure (Pa), D_a for the equilibrium diameter (m), D_m for the magnet disk diameter (m), D_o for the right dynamic ring outer diameter (m)

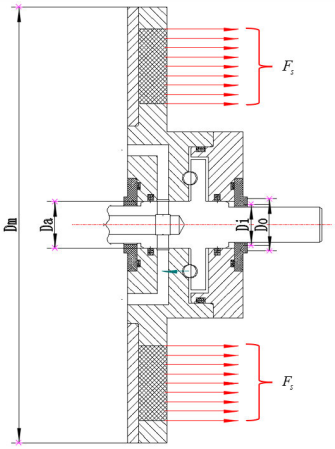

FIGURE 5. Conductor disk yoke electromagnetic force.

The magnet disk is subjected to the conductor disk yoke electromagnetic force F_s is:

$$F_s = \oint_{s_6} \overleftrightarrow{T_6}\, \mathrm{d}A_6 \tag{2}$$

where S_6 is the surface enclosing the periphery of the conductor disk yoke and $\overleftrightarrow{T_6}$ is the Maxwell tensor at that surface.

The magnet disk is subjected to the conductor disk copper disk axial electromagnetic force F_{z1} is:

$$F_{z_1} = \oint_{s_4} \overleftrightarrow{T_4}\, \mathrm{d}A_4 \tag{3}$$

where S_4 is the surface enclosing the periphery of the conductor disk yoke and $\overleftrightarrow{T_4}$ is the Maxwell tensor at that surface.

The magnet disk is subjected to a torque T of the conductor disk is:

$$T = \frac{P_{loss}}{\omega} \tag{4}$$

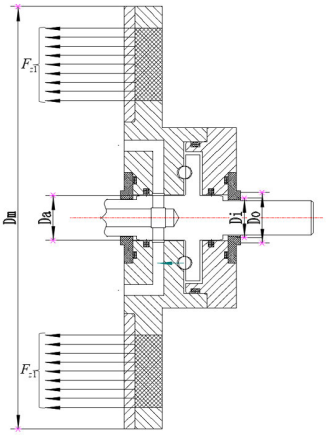

FIGURE 6. Conductor disk copper disk axial electromagnetic force.

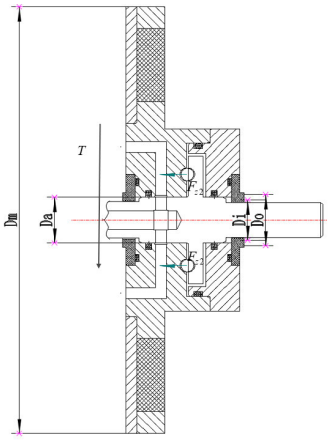

FIGURE 7. The axial force converted from the water supply shaft assembly (the ball cam force multiplier mechanism).

where P_{loss} is the eddy current loss of the conductor disk assembly during rotation, calculated from electromagnetic field analysis, and ω is the rotational speed difference between the conductor disk assembly and the magnet disk assembly.

The axial force F_{z_2} on the magnet disk assembly by the water supply shaft assembly (the ball cam force multiplier mechanism) is:

$$F_{z_2} = \kappa T \tag{5}$$

$$\kappa = \frac{1}{r_{ball} \cdot \tan\varphi} \tag{6}$$

where κ is the magnification of torque converted to axial force, r_{ball} is the radius of the distribution circle of the steel ball, φ is the inclination angle of the ball raceway along the circumferential expansion. The amplification of the force multiplication mechanism is shown in Fig.8.

The combined force F_p of the liquid film membrane pressure p on the sealing contact surface is:

$$F_p = \int_{D_i}^{D_o} p \cdot \frac{\pi}{2} d\,\mathrm{d}d \tag{7}$$

where $p = p_l \cdot (2D_0 + D_i)/3\,(D_0 + D_i)$

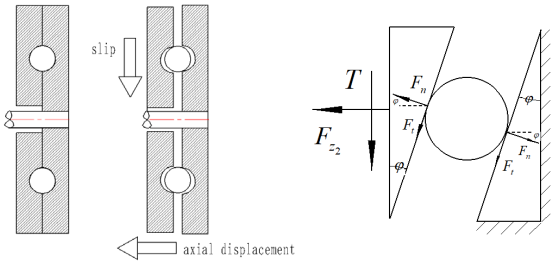

FIGURE 8. Expanded diagram of the principle of the ball cam force multiplier mechanism.

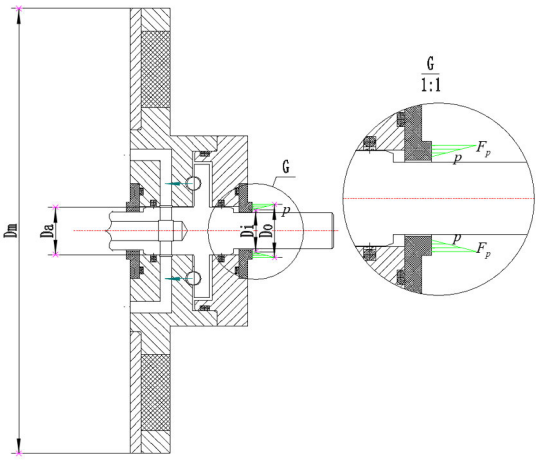

FIGURE 9. The combined force of the liquid film membrane pressure on the sealing contact surface.

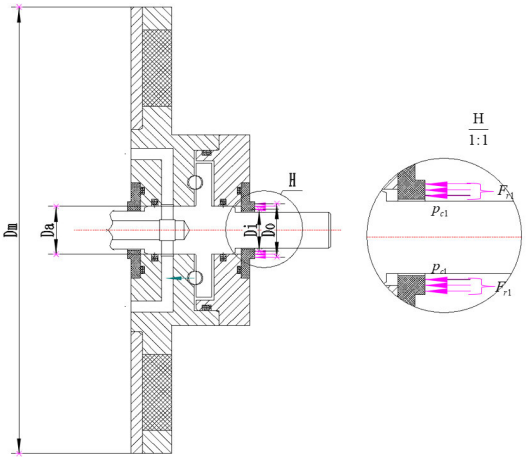

FIGURE 10. The bearing force of the micro-convex body of the sealing contact surface.

The combined force F_{r_1} on the micro-convex body at the seal face is:

$$F_{r_1} = \int_{D_i}^{D_o} p_{c_1} \cdot \frac{\pi}{2} d\mathrm{d}d \tag{8}$$

Thus, the equilibrium equation for the magnet disk assembly is:

$$F_{r_1} + F_{z_1} + F_{z_2} + F_p = F_l + F_s \tag{9}$$

Therefore, the end face specific pressure P_{c_1} of the seal under cylinder operating conditions is:

$$P_{c_1} = \frac{F_{r_1}}{A} = \frac{F_l + F_s - F_{z_1} - F_{z_2} - F_p}{A} \tag{10}$$

Expanding Eq. 9 yields:

$$F_p = \int_{D_i}^{D_o} p \cdot \frac{\pi}{2} d\mathrm{d}d \tag{11}$$

$$P_{c_1} = (K - \lambda)\, p_l + \frac{F_s - F_{z_1} - \kappa T}{A} \tag{12}$$

where, $k = \left(D_o^2 - D_a^2\right) / \left(D_o^2 - D_i^2\right)$ is the equilibrium coefficient; $\lambda = (2D_o + D_i) / (3\,(D_o + D_i))$ is the membrane pressure coefficient; $A = \left(\pi\left(D_o^2 - D_i^2\right)\right)/4$ is the seal ring contact area (m^2).

2) SPRAY WORKING CONDITION FORCE ANALYSIS

The right seal of the permanent magnet eddy current valve for the outer rotor under spraying condition is open and the left seal is closed, at this time, the forces on the end surface at the left seal include the combined force F_l of the hydraulic medium pressure on both ends of the magnet disk, the gravitational force F_s of the magnet disk by the yoke iron of the conductor disk, the electromagnetic force F_{z_1} of the conductor copper disk on the magnet disk, the axial force F_{z_2} transformed by the torque transmitted by the permanent magnet eddy current, the liquid film support force F_p on the sealing contact surface, and the micro-convex support force F_{r_2}.

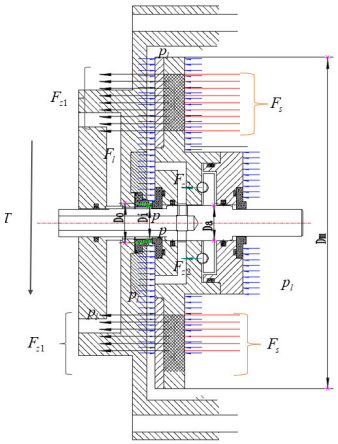

FIGURE 11. Spray working condition sealing force diagram.

The magnet disk is subjected to the combined force F_l of the fluid medium p_l in the sealing end face is:

$$F_l = \int_{D_a}^{D_m} p_l \cdot \frac{\pi}{2} d\mathrm{d}d - \int_{D_o}^{D_m} p_l \cdot \frac{\pi}{2} d\mathrm{d}d = \int_{D_a}^{D_o} p_l \cdot \frac{\pi}{2} d\mathrm{d}d \tag{13}$$

where p_l is the medium pressure (Pa), D_a is the equilibrium diameter (m), D_m is the diameter of the magnet disk (m), D_o is the outer diameter of the left moving ring (m)

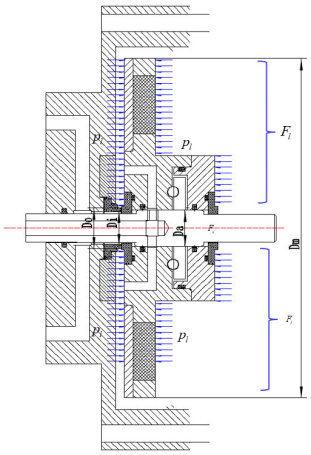

FIGURE 12. Fluid combined pressure.

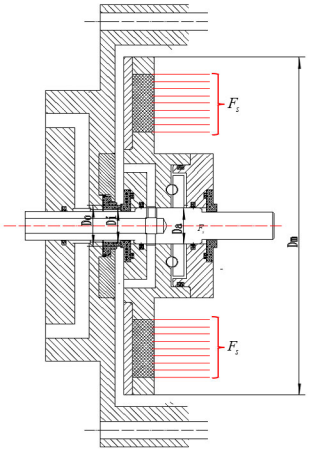

FIGURE 13. Conductor disk yoke electromagnetic force.

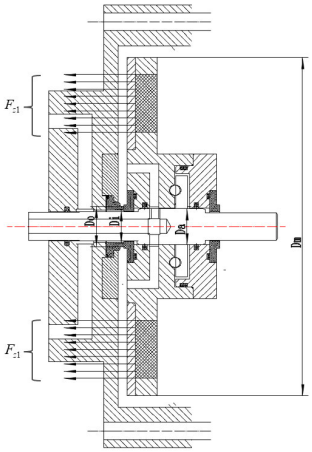

FIGURE 14. Conductor disk copper disk axial electromagnetic force.

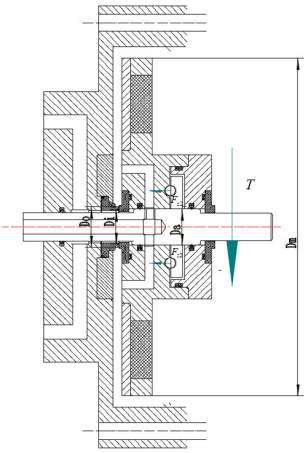

FIGURE 15. The axial force converted from the water supply shaft assembly (the ball cam force multiplier mechanism).

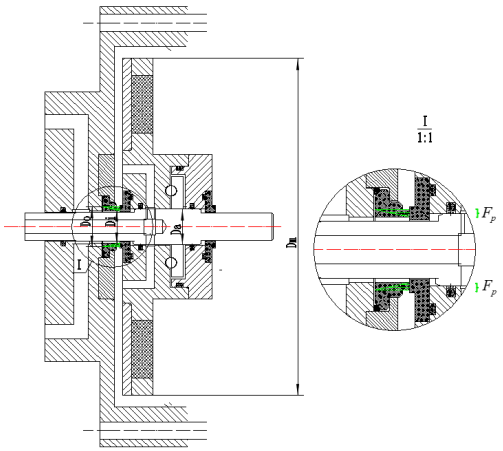

FIGURE 16. The combined force of the liquid film membrane pressure on the sealing contact surface.

Similarly, Eq. (2), Eq. (3), Eq. (4), Eq. (5), and Eq. (6) can be used to find electromagnetic force F_s on the magnet disk by the conductor disk yoke iron, the electromagnetic force F_{z_1} on the magnet disk by the conductor disk copper layer, the axial force F_{z_2} on the magnet disk by the water supply shaft, the combined force F_p of the liquid film membrane pressure p on the sealing contact surface.

Therefore, the combined force F_{r_2} on the micro-convex body at the seal end face is:

$$F_{r_2} = \int_{D_i}^{D_o} p \cdot \frac{\pi}{2} d\mathrm{d}d \tag{14}$$

Thus, the equilibrium equation for the magnet disk assembly is:

$$F_{r_2} + F_s + F_p = F_l + F_{z_1} + F_{z_2} \tag{15}$$

Therefore, the specific pressure P_{c_2} at the end face of the seal at the left of the spray condition is:

$$P_{c_2} = \frac{F_{r_2}}{A} = \frac{F_l + F_{z_1} + F_{z_2} - F_s - F_p}{A} \tag{16}$$

Expand to obtain:

$$P_{c_2} = (K - \lambda)p_l + \frac{F_{z_1} + \kappa T - F_s}{A} \tag{17}$$

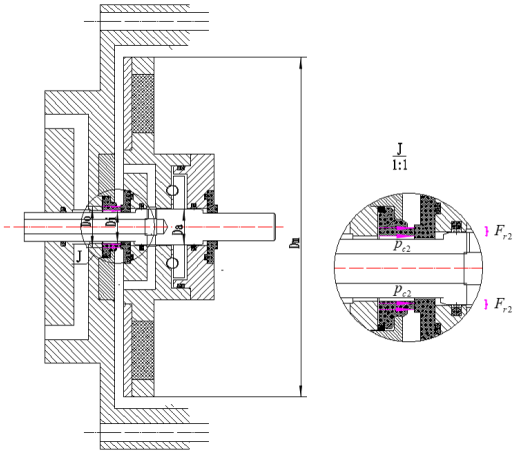

FIGURE 17. The bearing force of the micro-convex body of the sealing contact surface.

B. MECHANICAL SEALING CONDITIONS AND SWITCHING CONDITIONS OF PERMANENT MAGNET EDDY CURRENT SWITCHES UNDER DIFFERENT OPERATING CONDITIONS

The components of the right seal of the cylinder condition, the end face pressure P_{c1}, and the left seal of the spray condition, the end face pressure P_{c2}, show that the factors affecting the end face pressure P_c include the pressure of the sealing medium p_l, the equilibrium coefficient K, the membrane pressure coefficient λ, the coefficients κ related to the structural dimensions of the ball cam force multiplier mechanism, and the axial force F_s, F_{z_1} of the permanent magnetic coupling field, and the torque T of the permanent magnetic coupling field. According to the reference [15], it can be seen that in the end face pressure can be maintained at a maximum value $[P_c]_{\max}$ of 0.6MPa and a minimum value $[P_c]_{\min}$ of 0.3MPa. When the end face pressure exceeds $[P_c]_{\max}$, the sealing surface can fit properly, but the liquid film between the sealing end faces cannot be produced, resulting in substantial sealing surface wear and early seal failure. The end face pressure is less than $[P_c]_{\min}$, hence the seal is unstable and prone to leaking. In the left and right mechanical seal balance diameter D_a, balance coefficient K, sealing ring width b, and sealing medium pressure p_l to determine the case, the seal and open the compensating force by the permanent magnetic coupling field transfer of axial force and torque of the combined force F_{em} provide.

The end face compensation force F_{em1} of the right seal under cylinder condition is:

$$F_{em1} = F_s - F_{z_1} - \kappa T \tag{18}$$

The end face compensation force F_{em_2} of the right seal under cylinder condition is:

$$F_{em2} = F_{z_1} + \kappa T - F_s \tag{19}$$

The parameters of the mechanical seal structure of the permanent magnet vortex valve can be obtained by transforming the equilibrium coefficient according to reference [15]:

$$D_i = -2b\,(1-K) + \sqrt{D_a - 4b^2K\,(1-K)} \tag{20}$$

$$D_o = D_i + 2b \tag{21}$$

Therefore, in order to maintain the proper end face pressure during sealing, the end face compensation force F_{em1} provided by the permanent magnet coupling device is solved by Eq. (9), Eq. (15), Eq. (19), and Eq. (20):

$$F_{em1_{Close}} \leqslant \frac{1}{2}2b\pi\left([P_c]_{\max} - (K-\lambda)\,p_l\right) \cdot \left(2bK + \sqrt{D_a^2 - 4b^2K\,(1-K)}\right) \tag{22}$$

$$F_{em_{1Close}} \geqslant \frac{1}{2}b\pi\left([P_c]_{\min} - (K-\lambda)\,p_l\right) \cdot \left(2bK + \sqrt{D_a^2 - 4b^2K\,(1-K)}\right) \tag{23}$$

In the formula λ, the structural parameters of the seal, such as the balancing diameter D_a, the balancing coefficient K, and the seal ring width b, can be expressed as follows:

$$\lambda = \frac{6bK - 2b + 3\sqrt{D_a^2 - 4b^2K\,(1-K)}}{6\left(2bK - b + \sqrt{D_a^2 - 4b^2K\,(1-K)}\right)} \tag{24}$$

When the right seal needs to be opened under spraying condition, the end face specific pressure P needs to be reduced to 0. At this time, the end face compensation force F provided by the permanent magnet coupling device needs to be in the range as follows:

$$F_{em_{1Open}} \leq \frac{b\pi\,(K-\lambda)\,p_l \cdot \left(2bK + \sqrt{D_a^2 - 4b^2K\,(1-K)}\right)}{2} \tag{25}$$

Similarly, in order to maintain the proper end face pressure P_{c2} during sealing, the end face compensation force F_{em2} provided by the permanent magnet coupling device is solved by Eq. (13), Eq. (15), Eq. (19), and Eq. (20):

$$F_{em_{2Close}} \leq \frac{b\pi\left([P_c]_{\max} - (K-\lambda)\,p_l\right) \cdot \left(2bK + \sqrt{D_a^2 - 4b^2K\,(1-K)}\right)}{2} \tag{26}$$

$$F_{em_{2Close}} \geq \frac{b\pi\left([P_c]_{\min} - (K-\lambda)\,p_l\right) \cdot \left(2bK + \sqrt{D_a^2 - 4b^2K\,(1-K)}\right)}{2} \tag{27}$$

When it is necessary to open the left seal in spray or shutdown conditions, the end face pressure needs to be reduced to zero and the compensation force F_{em_2} provided by the permanent magnet coupling device is required:

$$F_{em_{2Open}} \leq \frac{b\pi\,(K-\lambda)\,p_l \cdot \left(2bK + \sqrt{D_a^2 - 4b^2K\,(1-K)}\right)}{2} \tag{28}$$

C. STRUCTURAL PARAMETER DESIGN OF MECHANICAL SEALS FOR PERMANENT MAGNET EDDY CURRENT SWITCHES

At this point, it can be concluded that in the permanent magnet eddy current valve two at the mechanical seal in the speed w can be normal sealing face compensation force $F_{em1_{Close}}$ and $F_{em2_{Close}}$ should be greater than to maintain the stability of the seal of the smallest end face pressure and less than to maintain the stability of the seal of the maximum end face pressure and seal switching to overcome the equilibrium of the liquid film pressure of the end face compensation force $F_{em1_{Open}}$ and $F_{em2_{Open}}$ should be satisfied with the relationship as follows:

$$\begin{cases} \left([p_c]_{\min} - (K-\lambda)\, p_l\right) A \le F_{em_{1Close}}(\omega) \\ \quad \le \left([p_c]_{\max} - (K-\lambda)\, p_l\right) A \\ F_{em_{1Open}}(\omega) \ge (K-\lambda)\, p_l A \\ \left([p_c]_{\min} - (K-\lambda)\, p_l\right) A \le F_{em_{2Close}}(\omega) \\ \quad \le \left([p_c]_{\max} - (K-\lambda)\, p_l\right) A \\ F_{em_{2Open}}(\omega) \ge (K-\lambda)\, p_l A \end{cases} \tag{29}$$

The transmission characteristics of the disk-type permanent magnet coupler are that the torque and axial force decrease with the increase of the air gap, at which point there are:

$$\begin{cases} F_{em_{1Close}}(\omega) > F_{em_{2Open}}(\omega) \\ F_{em_{1Open}}(\omega) > F_{em_{2Close}}(\omega) \end{cases} \tag{30}$$

That is to say, when the left seal of the spray condition can be opened, the right seal of the cylinder condition must be able to close stably after switching the condition; when the left seal of the spray condition can be closed, the right seal of the cylinder condition must be able to open stably before switching the condition.

$$\begin{cases} (K-\lambda)\, p_l A \le F_{em_{2Open}}(\omega) \le ([p_c]_{\max} \\ \quad - (K-\lambda)\, p_l) A \\ \left([p_c]_{\min} - (K-\lambda)\, p_l\right) A \le F_{em_{2Close}}(\omega) \\ \quad \le \left([p_c]_{\max} - (K-\lambda)\, p_l\right) A \end{cases} \tag{31}$$

IV. ANALYTICAL MODELING AND VALIDATION OF ELECTROMAGNETIC FIELDS IN PERMANENT MAGNET EDDY CURRENT SWITCHES

A. STRUCTURAL MODEL OF PERMANENT MAGNET COUPLING DEVICE FOR PERMANENT MAGNET EDDY CURRENT SWITCHES

The permanent magnet coupling device model of the permanent magnet eddy current switches for the external rotor is shown in Fig.18.

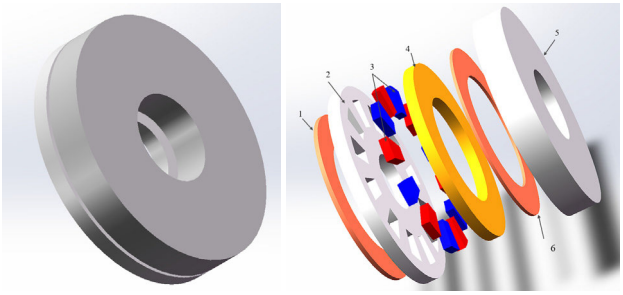

FIGURE 18. Model of permanent magnet coupling device for permanent magnet eddy current switches for outer rotor.

TABLE 3. Units for magnetic properties.

No.	subassembly	NO.	subassembly
1	Magnet Disk Backing-iron	4	Copper Disk
2	Non-magnetic stainless steel frame	5	Non-magnetic stainless steel frame
3	Permanent Magnet Array	6	conductor disk yoke iron

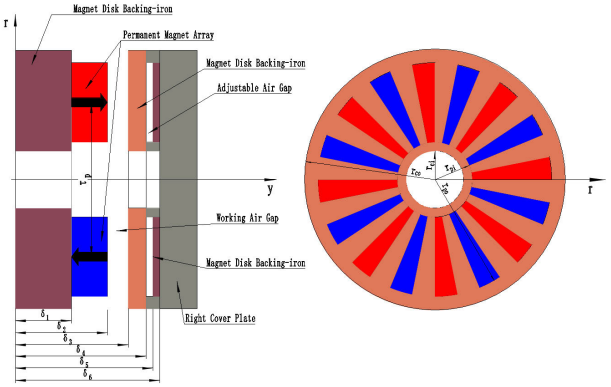

FIGURE 19. Structural model of permanent magnet coupling device for permanent magnet eddy current switches for outer rotor.

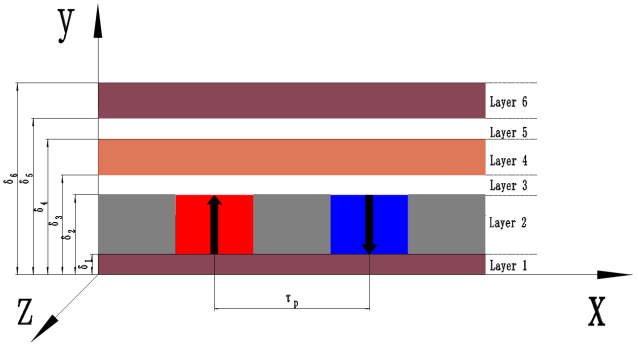

FIGURE 20. Two-dimensional linear hierarchical model of a permanent magnet coupling device in a right-angle coordinate system.

B. ANALYTICAL MODELING OF ELECTROMAGNETIC FIELDS IN PERMANENT MAGNET COUPLING DEVICES

1) MAGNETIC FIELD MODEL AND UNDERLYING ASSUMPTIONS

In order to simplify the calculation procedure and facilitate the study, we expand the model of the permanent magnet coupling device with permanent magnet eddy current switch for the outer rotor into a linear model along the circumferential direction, as shown in Fig.20, which can be obtained as a two-dimensional linear model in Cartesian coordinate

system. The transformed 2D linear model can be divided into different six layers:

Layer 1: magnet disk backing iron layer;
Layer 2: permanent magnet layer;
Layer 3: working air gap layer;
Layer 4: solid conductor layer;
Layer 5: adjustable air gap layer;
Layer 6: conductor disk yoke iron layer.

The following assumptions were made:

1) Only eddy current components in the z-direction are considered and the z-direction eddy current component subdomains x and y are correlated, since only the z-direction eddy current component contributes to the torque of the coupling device;
2) The layers are homogeneous with consistent material properties and the air region outside the two yoke iron layers is not considered;
3) The curvature error due to the transformation of the coordinate system is neglected;
4) The model has a natural period boundary condition along the x-direction and the period is determined by the pole spacing of the permanent magnets;
5) The yoke iron on the conductor disk assembly has a finite permeability μ_6 and a non-zero conductivity σ_6, Eddy current effects in this layer should be considered in the layer model;
6) Displacement currents in the conductor are neglected;
7) Use the relative velocity between the conductor disk and the magnet disk for the analysis. The relative velocity v can be expressed as:

$$v = \frac{2\pi n R_{avg}}{60} \tag{32}$$

where n is the rotational speed of the conductor disk with the cylinder in rpm; R_{avg} is the average radius of the permanent magnet in meter, and R_{avg} can be calculated by $R_{avg} = (r_{pi} + r_{po})/2$.

2) BASIC CONTROL EQUATIONS OF MAGNETIC FIELD AND VECTOR MAGNETIC POTENTIAL DISTRIBUTION

Based on reference [14] and [16], the basic equation for the magnetic field of the disk-type permanent magnet coupling device of the permanent magnet eddy current switch is expressed in terms of the magnetic vector as:

$$\nabla^2 \mathbf{A}_k = -\mu_0 (\mu_k \nabla \times \mathbf{H}_k + \nabla \times \mathbf{M}_k) \tag{33}$$

where $\mathbf{A}_k$ is the magnetic vector of layer k; μ_0 is the vacuum permeability and its value is $4\pi \times 10^{-7}$ H/m; μ_k is the relative permeability of layer k; $\mathbf{H}_k$ is the magnetic field strength of layer k; $\mathbf{M}_k$ is the magnetization strength of layer k.

In the layer 2, there is a field source but no current, which excites a magnetic field $\mathbf{M}_2 = \mathbf{M}_r$, with the following magnetic induction in the x and y directions:

$$\mathbf{B}_2 = \begin{bmatrix} B_{2,x} \\ B_{2,y} \end{bmatrix} = \mu_0 \mu_2 \begin{bmatrix} H_{2,x} \\ H_{2,y} \end{bmatrix} + \mu_0 \begin{bmatrix} 0 \\ M_r \end{bmatrix} \tag{34}$$

After determining the permanent magnet material of a fixed model, the relationship between the magnetization strength $\mathbf{B}_r$ of the permanent magnet and the residual magnetization strength $\mathbf{M}_r$ of the permanent magnet can be expressed as follows:

$$\mathbf{M}_r = \frac{\mathbf{B}_r}{\mu_0} \tag{35}$$

as a result:

$$\nabla \times \mathbf{B}_2 = \nabla \times (\mathbf{H}_2 + \mathbf{M}_r) = \mu_0 \nabla \times \mathbf{M}_r \tag{36}$$

The field control equation satisfied by Layer 2 is:

$$\nabla^2 \mathbf{A}_2 = -\mu_0 \nabla \times \mathbf{M}_r = -\nabla \times \mathbf{B}_2 \tag{37}$$

Layer 1,3,5 has neither a field source nor a current, with equation (37):

$$\begin{cases} \nabla \times \mathbf{H}_k = \mathbf{J}_k = 0 \\ \mathbf{B}_k = \mu_0 \mathbf{H}_k \end{cases} \tag{38}$$

The field control equations satisfied by Layers 1,3and5 are:

$$\nabla^2 \mathbf{A}_k = 0 \quad k = 1, 3, 5 \tag{39}$$

Layers 4 and 6 do not have a field source, but they do have a current.:

$$\begin{cases} \nabla \times \mathbf{H}_k = \mathbf{J}_k \\ \mathbf{J}_k = \sigma_k \mathbf{E}_k \\ \nabla \times \mathbf{E}_k = -\dfrac{\mathrm{d}\mathbf{B}_k}{\mathrm{dt}} = -\dfrac{\mathrm{d}\mathbf{B}_k}{\mathrm{d}x}\dfrac{\mathrm{d}x}{\mathrm{dt}} = -\dfrac{\mathrm{d}\mathbf{B}_k}{\mathrm{d}x} v \\ \mathbf{B}_k = \mu_0 \mu_k \mathbf{H}_k \end{cases} \tag{40}$$

So the field control equations satisfied by Layers 4,6 are:

$$\nabla^2 \mathbf{A}_k = \mu_0 \mu_k \frac{\partial \mathbf{A}_k}{\partial x} \, k = 1, 3, 5 \tag{41}$$

By solving (37), (39), and (41), the vector magnetic potential of each layer can be obtained as follows:

$$\begin{cases} \mathbf{A}_1 = (C_1 e^{my} + D_1 e^{-my}) e^{-jmp\theta} \\ \mathbf{A}_2 = (C_2 e^{my} + D_2 e^{-my} - \frac{jB_r}{m}) e^{-jmp\theta} \\ \mathbf{A}_3 = (C_3 e^{my} + D_3 e^{-my}) e^{-jmp\theta} \\ \mathbf{A}_4 = (C_4 e^{\lambda_4 y} + D_4 e^{-\lambda_4 y}) e^{-jmp\theta} \\ \mathbf{A}_5 = (C_5 e^{my} + D_5 e^{-my}) e^{-jmp\theta} \\ \mathbf{A}_6 = (C_6 e^{\lambda_6 y} + D_6 e^{-\lambda_6 y}) e^{-jmp\theta} \end{cases} \tag{42}$$

In (41), the coefficients C_k and D_k are derived using the model boundary conditions, and λ is calculated using the open square calculation of complex numbers [17]:

$$\begin{cases} \lambda_i = \sqrt[4]{m^4 + (m\mu_0\mu_i\sigma_i v)^2} e^{\xi_i} \\ \xi_i = \dfrac{i}{2} \arctan\left(\dfrac{\mu_0 \mu_i \sigma_i v}{m}\right) \end{cases} \quad i = 4, 6 \tag{43}$$

3) BOUNDARY AND INTERFACE CONDITIONS

From the assumption 2 that the region beyond the two-sided yoke iron is not considered, the boundary condition imposed on the layer model is:

$$\begin{cases} \dfrac{\partial \mathbf{A}_{1n}}{\partial x}\Big|_{y=0} = 0 \\ \dfrac{\partial \mathbf{A}_{6n}}{\partial x}\Big|_{y=\delta_6} = 0 \end{cases} \tag{44}$$

According to the basic theory of electromagnetic fields, the magnetic field at the interface of different media satisfies the continuity of the tangential component of the magnetic field strength and the continuity of the normal component of the magnetic induction strength (which satisfies the Delicacy-Neumann interface condition).

$$\frac{d\mathbf{A}_{kn}}{dx} = \frac{d\mathbf{A}_{(k+1)n}}{dx}\Big|_{y=\delta_k} \quad k = 1, 2, 3, 4, 5 \tag{45}$$

$$\frac{1}{\mu_k}\frac{d\mathbf{A}_{kn}}{dy} = \frac{1}{\mu_{k+1}}\frac{d\mathbf{A}_{(k+1)n}}{dy}\Big|_{y=\delta_k} \quad k = 1, 2, 3, 4, 5 \tag{46}$$

where δ_k are the y-coordinates of the interfaces of the layers in the layer model, as is shown in Fig.19 and Fig.20, the values of which are determined by the structural parameters of the disk-type permanent magnet coupling device.

Appendix shows the detailed form of the boundary conditions.

4) EDDY CURRENT LOSS AND TORQUE EQUATION

From the relationship between the eddy current density and the magnetic vector, the expression for the eddy current density in the copper conductor disk and the yoke iron in the conductor disk assembly can be obtained as

$$J_{4z} = -\sigma_4 v\frac{\partial \mathbf{A}_4}{\partial x} \tag{47}$$

$$J_{6z} = -\sigma_6 v\frac{\partial \mathbf{A}_6}{\partial x} \tag{48}$$

Thus, the average eddy current density of the copper conductor disk and the yoke iron in the conductor disk assembly can be expressed as:

$$J_{4avg} = \frac{\int_{\delta_3}^{\delta_4}\int_{-\tau_p/2}^{\tau_p/2} J_{4z}dxdy}{\tau_p\left(\delta_4 - \delta_3\right)} \tag{49}$$

$$J_{6avg} = \frac{\int_{\delta_5}^{\delta_6}\int_{-\tau_p/2}^{\tau_p/2} J_{6z}dxdy}{\tau_p\left(\delta_6 - \delta_5\right)} \tag{50}$$

The eddy current loss of the copper conductor disk and the yoke iron in the conductor disk assembly are calculated from the eddy current density as:

$$P_{4\omega} = \frac{L_4}{\sigma_4}\int\int_{Layer4}\left|J_{4avg}^2\right|dxdy \tag{51}$$

$$P_{6\omega} = \frac{L_6}{\sigma_6}\int\int_{Layer6}\left|J_{6avg}^2\right|dxdy \tag{52}$$

The analytical expression for the output torque of the entire conductor disk assembly as:

$$T = \frac{P_{4\omega} + P_{6\omega}}{\omega} \tag{53}$$

The induced eddy currents in the conductive layer of the conductor disk assembly are present in the conductive layer in a closed-loop form, but only the eddy currents flowing along the radial direction affect the torque of the disk-type permanent magnet coupling device for the permanent magnet eddy current switch for the outer rotor. Therefore, Eq. (53) ignores the circumferential flow of eddy currents outside the region directly opposite to the permanent magnet and conductor disk, so the calculated torque is biased compared with the actual situation, and a three-dimensional correction for end effects can make the model calculation results more closely match the actual situation. Reference [17] R-N correction factor provides a correction factor considering the three-dimensional end effect, which improves the accuracy of the torque calculation of the model.

$$k_s = 1 - \frac{\tanh\left(\frac{\pi\delta_p}{2\tau_p}\right)}{\frac{\pi\delta_p}{2\tau_p}\left\{1 + \tanh\left(\frac{\pi\delta_p}{2\tau_p}\right)\tanh\left(\frac{\pi\left(\delta_c - \delta_p\right)}{2\tau_p}\right)\right\}} \tag{54}$$

where δ_p represents the permanent magnet's radial length, $\delta_p = r_{po} - r_{pi}$, whereas δ_c represents the copper disc's radial width, $\delta_c = r_{co} - r_{ci}$. τ_p is the pole-angle spacing between adjacent permanent magnets of the magnet disk.

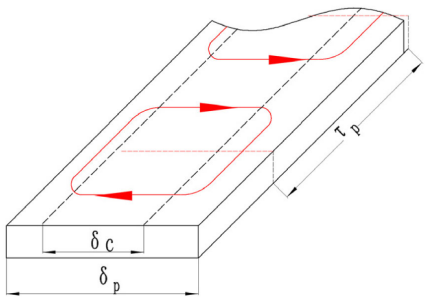

FIGURE 21. The real eddy current direction of the copper disc.

The model of the output torque after considering the three-dimensional eddy current effect is expressed as:

$$T_o = k_s T \tag{55}$$

5) EQUATIONAXIAL FORCE FORMULA

Based on the relationship between the magnetic vector and the magnetic density, the analytical expressions for the x-direction (circumferential) and y-direction (axial) components of the magnetic density in each layer can be obtained as:

$$B_{4x} = \frac{\partial \mathbf{A}_4}{\partial y}, B_{6x} = \frac{\partial \mathbf{A}_6}{\partial y} \tag{56}$$

$$B_{4y} = \frac{\partial \mathbf{A}_4}{\partial x}, B_{6y} = \frac{\partial \mathbf{A}_6}{\partial x} \tag{57}$$

The axial force on the magnet disk can be expressed according to the Maxwell tensor method, and the axial force can be expressed as:

$$F_y = \oiint_{S_4} \vec{T} \cdot ds + \oiint_{S_6} \vec{T} \cdot ds \tag{58}$$

where S_4 is the surface enclosing the copper disk, is the surface enclosing the yoke iron of the conductor disk $\overleftrightarrow{T}$ is the Maxwell stress tensor at any point on the surface. The permanent magnet eddy current switches electromagnetic field model of the surface of the conductor disk current density vector does not have an axial component, so the Maxwell tensor in the omission of the electric field strength term after the expression of the form shown in equation (59):

$$\overleftrightarrow{T} = \frac{1}{\mu_0}\begin{bmatrix} B_x^2 - \frac{1}{2}|\mathbf{B}|^2 & B_xB_y & 0 \\ B_yB_x & B_y^2 - \frac{1}{2}|\mathbf{B}|^2 & 0 \\ 0 & 0 & -\frac{1}{2}|\mathbf{B}|^2 \end{bmatrix} \tag{59}$$

Therefore, the axial force provided by the fourth copper conductor layer is

$$F_{y4} = \frac{1}{\mu_0}\int_c^d \int_0^{2\pi r_{avg}} \left(\frac{\partial\left(B_{4y}B_{4x}\right)}{\partial y} + \frac{\partial\left(B_{4y}^2 - \frac{1}{2}|\mathrm{B}_4|^2\right)}{\partial y} \right) dxdy \tag{60}$$

Therefore, the axial force provided by the sixth conductor disk yoke iron is

$$F_{y6} = \frac{1}{\mu_0}\int_e^f \int_0^{2\pi r_{avg}} \left(\frac{\partial\left(B_{6y}B_{6x}\right)}{\partial y} + \frac{\partial\left(B_{6y}^2 - \frac{1}{2}|\mathrm{B}_6|^2\right)}{\partial y} \right) dxdy \tag{61}$$

Therefore, the axial force F_{em} on the magnet disc assembly is:

$$F_{em} = F_y + \kappa T \tag{62}$$

C. FINITE ELEMENT ANALYSIS OF ELECTROMAGNETIC FIELD OF PERMANENT MAGNET EDDY CURRENT DEVICE

In order to verify the validity of the two-dimensional analytical model proposed in the paper, the permanent magnet coupling device is analyzed by simulation verification. Here, the analytical expression models of the axial force and torque on the magnet disk are validated respectively, and the simulation results of the 3D finite element simulation are calibrated as the benchmark values for comparison.

1) DESCRIPTION OF STRUCTURAL PARAMETERS

In order to verify the accuracy of the analytical model of the electromagnetic field of the disk-type permanent magnet coupling device for permanent magnet eddy current switching. A three-dimensional finite element analysis was carried out according to the specifications of the disk-type permanent magnet coupling structure given in Tables 4 and 5.

TABLE 4. Parameters of permanent magnet coupling structure.

Symbol	Definition	Values
r_{pi}	Permanent magnet inner radius	160 mm
r_{po}	Permanent magnet outer radius	240 mm
r_{avg}	Radius of permanent magnet distribution circle	200 mm
r_{ci}	Copper conductor disk inner radius	70 mm
r_{co}	Copper conductor disk outer radius	130 mm
δ_{a1}	Thickness of first air gap	2 mm
δ_{a2}	Thickness of second air gap	10 mm
δ_1	First boundary thickness	6 mm
δ_2	Second layer boundary thickness	18 mm
δ_3	Third layer boundary thickness	20 mm
δ_4	Fourth layer boundary thickness	35 mm
δ_5	Fifth Boundary Thickness	45 mm
δ_6	Sixth Layer Boundary Thickness	49 mm
α	Permanent magnet duty cycle	0.5
p	Number of pole pairs	6
n	Difference in rotational speed	0~1500rpm
κ	Incremental force ratio	30

TABLE 5. Permanent magnet coupling device Material properties.

Symbol	Definition	Values
μ_0	Permeability of vacuum	$4\pi\times10^{-7}$ Tm/A
μ_1, μ_6	Relative permeability of magnet disk backing iron to conductor disk yoke iron (1008 steel)	2000
μ_4	Relative permeability of copper conductor layer (Copper)	0.999991
μ_3, μ_5	Relative permeability of the first air-gap layer to the second air-gap layer (air)	1
μ_2	Relative permeability of the permanent magnet layer (NdFeB35)	1.0997785406
H_c	Residual magnetism of permanent magnets (NdFeB35)	-8.9×10^5 A/m
B_r	Relative permeability of the inner yoke iron layer (1008 steel)	1.22 T
σ_4	Conductivity of copper conductor layer (Cu)	$5.7\text{x}10^7$ S/m
σ_6	Conductivity of conductor disk yoke iron (1008 steel)	$2.0\text{x}10^6$ S/m

2) SENSITIVITY ANALYSIS ON KEY PARAMETERS

The transmission characteristics of the permanent magnet coupling device were simulated by adjusting the duty cycle of the permanent magnet. With other parameters unchanged, the simulation results were shown in Fig.22 and Fig.23. The duty cycle of a permanent magnet is defined as the ratio of the total length of the permanent magnet to the total length of the distribution circle at the circumference of the mean radius of the permanent magnet.

These figures show that increasing the duty cycle of the permanent magnets significantly increases the static gravitational force (see Fig. 23) while simultaneously increasing the torque reversal point (see Fig. 22), resulting in a steeper overall transmission characteristic curve. After a duty cycle of more than 90%, there is no substantial change in transmission characteristics because the rise in magnetomotive potential changes synchronously for static gravitational force and repulsive force in the presence of a rotative speed difference. Under the full evaluation of static gravitational force

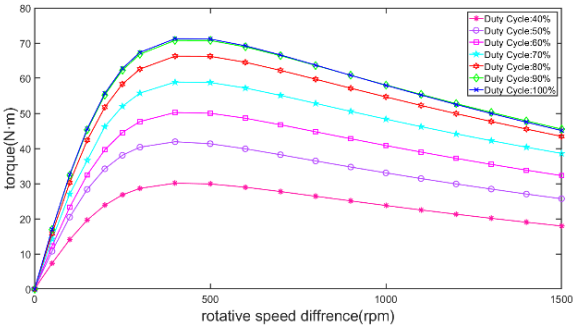

FIGURE 22. Torque characteristic curve of permanent magnet coupling structure with duty cycle.

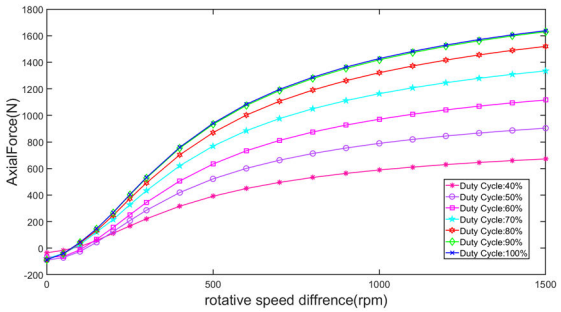

FIGURE 23. Axial force characteristic curve of permanent magnet coupling structure with duty cycle.

and transmission properties, it is more acceptable to retain the duty cycle of the permanent magnet between 50% and 70%, and in this design, 50% is chosen.

The transmission properties of the permanent magnet coupling device are simulated using different thicknesses of permanent magnets (6mm-15mm). Fig.24 and Fig.25 demonstrate the simulation findings. When the thickness of the permanent magnet is too small, the axial force on the magnet disc assembly cannot be detached, and the seal cannot be opened; however, increasing the thickness of the permanent magnet can significantly increase the static gravitational force, and at the same time, with the increase of the rotational speed difference, the corresponding axial repulsive force and torque reversal point will also increase, so that the transmission characteristic curve is steep.

In the example of this paper, when the thickness of the permanent magnet increases, the static gravitational attraction will gradually increase, and at the same time, the axial repulsion and torque under the same rotational speed difference will also increase, which will make the opening speed of the switch mechanical seal change. The thickness of the permanent magnet is finally selected as 12mm.

Under the premise of ensuring that the duty cycle of the permanent magnets remains unchanged, the simulation experiments are carried out by changing the number of permanent magnet pole-pairs, and the results are shown in Fig.26 and Fig.25. With the increase in the number of poles of the permanent magnets, the spacing between poles is shortened, and the leakage magnetism of the neighboring poles from the

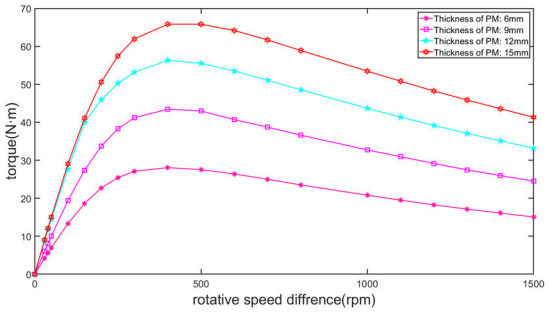

FIGURE 24. Torque force characteristic curve of permanent magnet coupling structure with permanent magnet thickness.

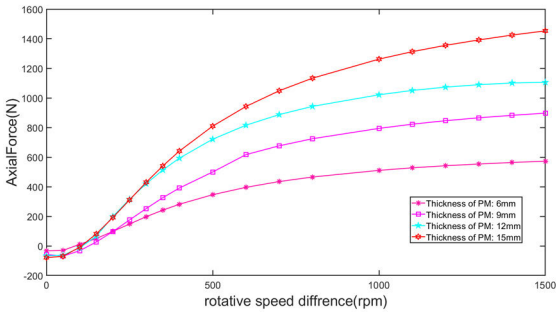

FIGURE 25. Axial force characteristic curve of permanent magnet coupling structure with permanent magnet thickness.

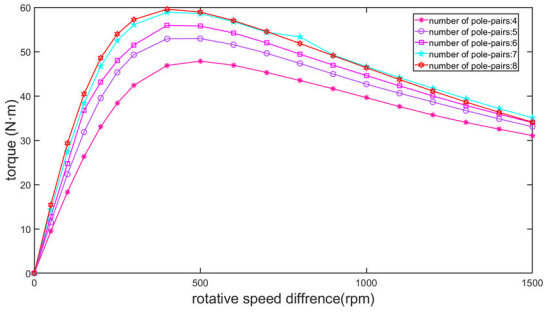

FIGURE 26. Torque force characteristic curve of permanent magnet coupling structure with number of pole-pairs.

poles and back to the poles through the air gap is increased, and the reduction of the magnetic kinetic potential of the main circuit reduces the axial gravitational force of the static state, and the scale of the induced eddy currents is weakened at the same time, so that the transmission characteristics of the axial force are more level.

However, as the number of permanent magnet pole pairs increases, the reversal points of the torque characteristic that can be transmitted by a permanent magnet coupled structure increases, making the curve of the torque characteristic steeper.

The actual design, in the case of structural allowances, according to the requirements of the mechanical seal switches on the axial force to select the number of pole pairs of magnets, but must ensure that sufficient distance between adjacent poles to prevent excessive magnetic leakage, in this

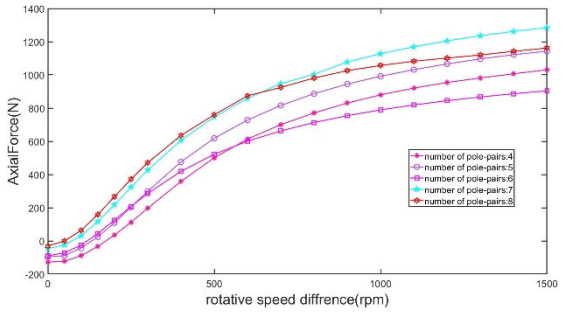

FIGURE 27. Axial force characteristic curve of permanent magnet coupling structure with number of pole-pairs.

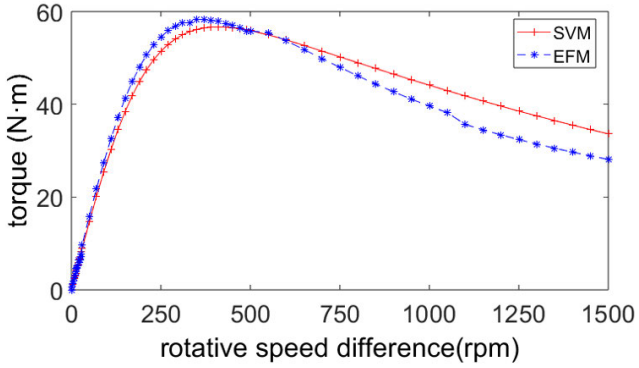

FIGURE 28. Torque characteristic curve of permanent magnet coupling device (cylinder working condition).

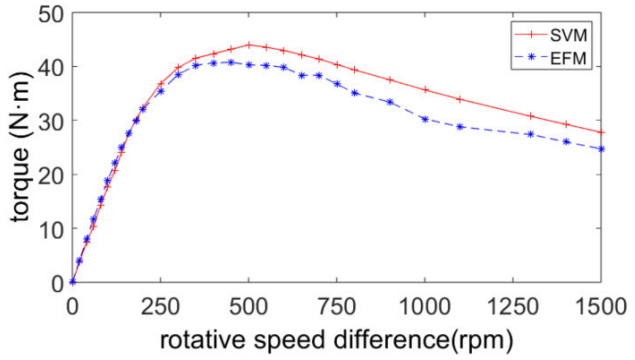

FIGURE 29. Torque characteristic curve of permanent magnet coupling device (spray condition).

example, the final take the number of pole pairs of permanent magnets for 6.

3) COMPARISON OF FINITE ELEMENT RESULTS WITH ANALYTICAL MODELLING RESULTS

Based on the initial parameters of 1) and the sensitivity analysis of the structural parameters of 2), the results of the finite element analysis are compared with the solution results of the layer model based on the method of separated variables in Section B, respectively, and the results are shown in Fig. 28 to Fig. 31.

The overall theoretical curves fit the finite element conclusions with good agreement in the low slip region. The

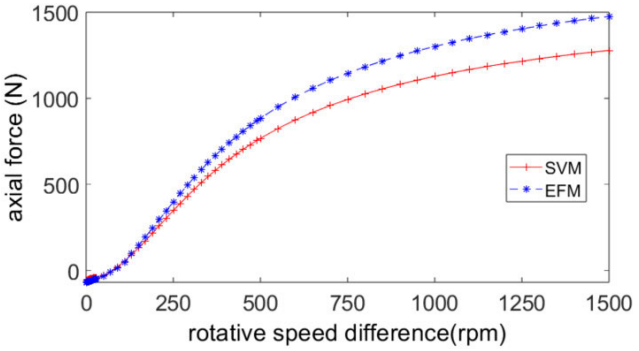

FIGURE 30. Axial force characteristic curve of permanent magnet coupling device (cylinder working condition).

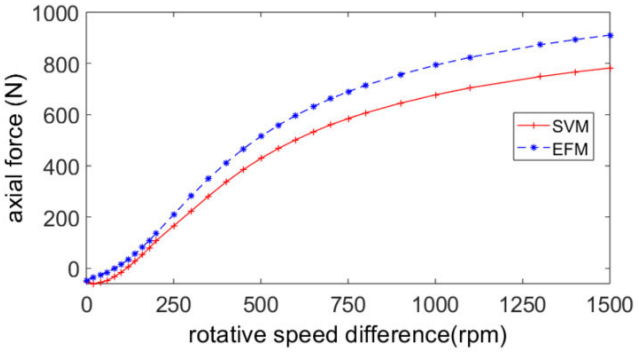

FIGURE 31. Axial force characteristic curve of permanent magnet coupling device (spray condition).

prediction results of the analytical modeling method are more accurate in the small slip region, and there is a large error in the larger slip region, but the trend of the torque curve is accurate. This is due to the fact that the R-N correction factor used in Section IV is particularly effective for low turnout cases, and errors occur when turnout is large. While the rotational speed of the cutting section of the coal mining cutting head is about 20 rpm when it is working, the analytical model can be used for the calculation of axial force and torque of the permanent magnet coupling device of the permanent magnet eddy current switches.

V. EXAMPLE OF MECHANICAL SEAL PERFORMANCE OF PERMANENT MAGNET EDDY CURRENT SWITCHES

A. SEALING CAPABILITY ANALYSIS

From the permanent magnetic coupling device electromagnetic field model calculations can be seen, so in the balance of the diameter D_a of 0.025m, the width of the sealing ring for 3mm, the balance coefficient K is 0.53, the sealing medium pressure for 3Mpa when the sealing of the compensating force as follows:

$$\begin{cases} F_{em1}\ (n=0, \delta_3-\delta_2=2\text{mm}) = 71.612\text{N} \\ F_{em2}\ (n=0, \delta_3-\delta_2=4\text{mm}) = -51.015\text{N} \\ F_{em2}\ (n=20\,\text{rpm}, \delta_3-\delta_2=4\text{mm}) = 71.935\text{N} \end{cases} \tag{63}$$

The end face pressure as follows:

$$\begin{cases} p_{c1}\,(n=0,\delta_3-\delta_2=2\text{mm})=0.3334\text{MPa} \\ p_{c2}\,(n=20\,\text{rpm},\delta_3-\delta_2=4\text{mm})=0.3348\text{MPa} \end{cases} \tag{64}$$

It can be concluded that the end face specific pressure of the right seal in the cylinder condition is 0.3334MPa, which meets the requirement of the end face specific pressure for sealing; at 20 rpm, the right seal in the cylinder condition can be opened stably and switched to the spraying condition, and the left seal in the spraying condition at this time is 0.3348MPa, which meets the requirement of the end face specific pressure for sealing.

At the time of shutdown, the compensating force provided by the permanent magnetic coupling device can overcome the pressure of the liquid and complete the opening of the left seal and the closing of the right seal in the spray condition. And the switching condition of the seal is:

$$\begin{cases} (K-\lambda)\,p_l A - F_{em1}\,(n,\delta_3-\delta_2=2\text{mm}) \le 0 \\ (K-\lambda)\,p_l A - F_{em2}\,(n,\delta_3-\delta_2=4\text{mm}) \le 0 \end{cases} \tag{65}$$

That is, when the end face specific pressure of the seal is less than or equal to 0, the closing force of the seal is not enough to overcome the opening force of the seal, and the seal will open at this time. It is calculated that under this set of sealing conditions, the right seal opens at speeds higher than 6.6 rpm and the left seal opens at speeds lower than 7.9 rpm.

B. LEAKAGE AND FRICTION ANALYSIS

1) FRICTION STATE JUDGMENT

In order to further determine the end face friction state of the mechanical seal, the working condition parameter G in reference [18] is used as a judgment criterion. The service condition parameter G is a similar quasi-count of the tribological properties of mechanical seals, which is the ratio of the viscous force of the fluid film between the end faces to the total load carrying capacity W, which can characterize the service condition of the seal and the load carrying capacity of the fluid film.

$$G=\frac{\mu n}{60P_c} \tag{66}$$

where μ is the hydrodynamic viscosity in $N\cdot s/m^2$; n is the rotational speed in *rpm*; and P_c is the specific pressure of the seal end face in pa.

The working condition parameter G of the mechanical seal of the permanent magnet eddy current switches can be obtained from Eq. (9) and Eq. (13) as follows

$$G_1=\frac{\mu n}{60\left((K-\lambda)\,p_l+\frac{F_{em_1}}{A}\right)} \tag{67}$$

$$G_2=\frac{\mu n}{60\left((K-\lambda)\,p_l+\frac{F_{em_2}}{A}\right)} \tag{68}$$

TABLE 6. Units for magnetic properties.

Friction state	G-value
Fluid Friction	>1x10-6
Combined Friction,	5x10-8~1x10-6
Boundary Friction	2x10-8~5x10-8

Eq. (67) and Eq. (68) are the working condition parameters of the right seal and the left seal, respectively. By the G value to determine the mechanical seal end face friction state based on Table 6 shows, you can roughly determine the design of the mechanical seal end face friction state.

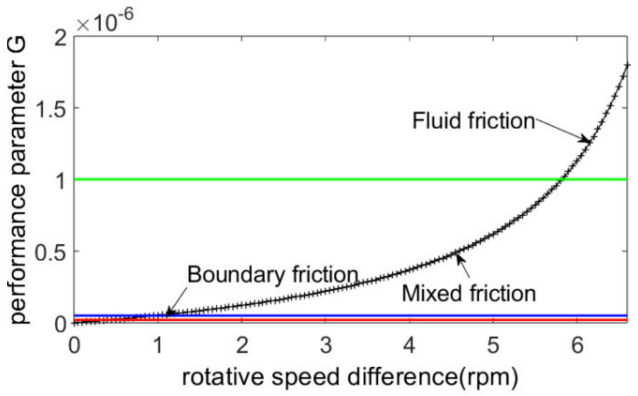

FIGURE 32. Sealing condition parameters for left conditions G.

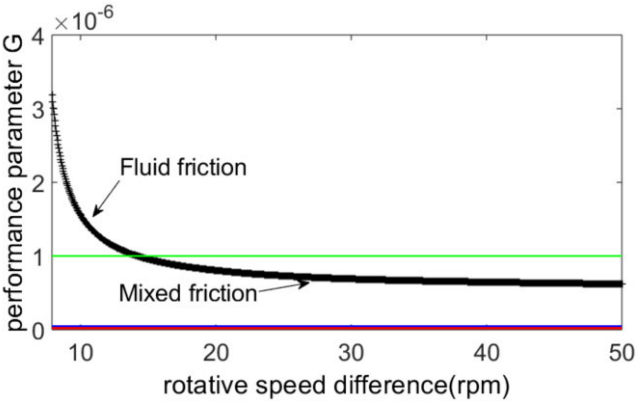

FIGURE 33. Sealing condition parameters for right conditions G.

From the previous calculations, it can be seen that between 2.0Mpa∼4.0MPa, the working condition parameter G of the right seal is shown in Fig.32, and the working condition parameter G of the left seal is shown in Fig.33.

Under the cylinder condition, the right seal is in boundary friction at 0∼1rpm, mixed friction at 1rpm∼5.8rpm, and fluid friction at 5.8rpm ∼6.6rpm; under the spray condition, the left seal is in fluid friction at 7.9rpm∼14.5rpm, and mixed friction at 14.5rpm∼50rpm.

2) LEAKAGE ANALYSIS

When the seal end face is in fluid lubrication, the leakage Q_c of the seal at this time is according to reference [18] as:

$$Q_c = \frac{\pi k D_o C_e^2 (p_2 - p_1)}{p_c^2} \tag{69}$$

where k is an empirical coefficient with a value of 3.3×105 in $\mathrm{kg \cdot cm^{-2} \cdot s^{-1}}$, p_2 is the pressure of the sealing medium; p_1 is the atmospheric pressure; C_e is the sealing surface gap, and according to reference [14] and [18], there are $C_e = 0.746R_{y_1} + R_{y_2}$, R_{y_1} is the maximum height of the contour of the surface of the moving ring, and R_{y_2} is the maximum height of the contour of the surface of the static ring.

When the seal end face is in a mixed friction state, the leakage of the seal Q_c is according to reference [18] as:

$$Q_c = 7.5 \times 10^{-15} (D_o + D_i)^3 n^{1.9} \cdot \eta^{-0.1} \left(K + \frac{F_{em}}{\Delta p}\right)^{-0.9} \Delta p^{0.1} \left(\ln\left(\frac{D_o}{D_i}\right)\right)^{-1} \tag{70}$$

where $\Delta p = (p_2 - p_1)$ is the system differential pressure in 0.1MPa.

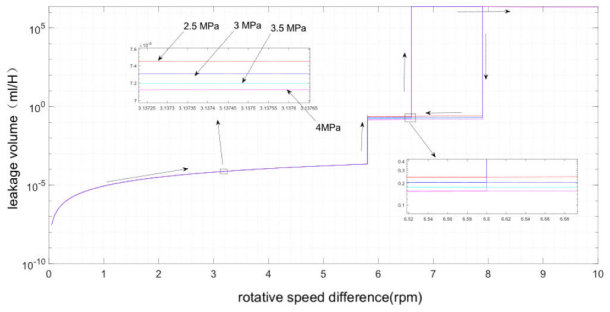

FIGURE 34. Leakage of seals Q_c at cylinder condition with speeds Schematic diagrams.

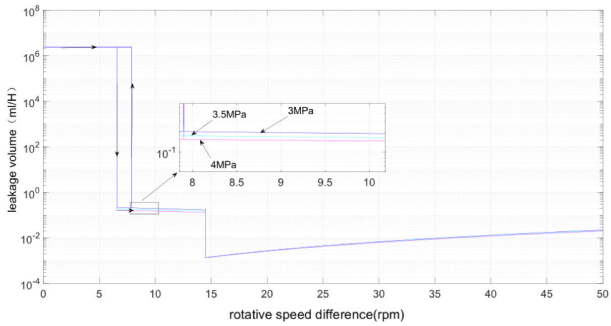

FIGURE 35. Leakage of seals Q_c spray condition with speeds Schematic diagrams.

It can be seen that the relationship between the leakage of the right seal in the cylinder condition and the left seal in the spray condition Q_c and the rotational speed n is shown in the figure.

In the range of 0∼50 rpm, under the fluid supply pressure of 2.0MPa∼4.0MPa, the leakage of the right sealing surface before it opens increases with the increase of rotational speed, but the maximum leakage is not more than 0.192mL/h, and the sealing end face opens when the rotational speed is more than 6.6rpm, and at this time, the leakage is 2.4×10^6mL/h. Under the fluid friction state, the leakage of the left sealing surface increases with the rotational speed and decreases. In the state of fluid friction, the leakage of the left sealing surface decreases with the increase of rotational speed, in the state of mixed friction, the leakage of the left sealing surface increases with the increase of rotational speed, but the highest does not exceed 0.2 mL/h. However, in the case of normal operation of the seal, even if the rotational speed is reduced to 10 rpm, in the case of the medium pressure of 2 MPa, the maximum leakage is not more than 0.280 mL/h, and the sealing end face opens at a low rotational speed, and at this time, the leakage is 2.4×10^6mL/h. Considering the end face specific pressure should be in the appropriate interval, the speed should not exceed 28 rpm, at this time in the liquid supply pressure of 2.0 MPa ∼ 4.0 MPa interval, can meet the sealing condition of switching as well as less than the average leakage stipulated 3mL/h in reference [15].

VI. RESULTS AND DISCUSSION

In this paper, a mechanical seal switch based on the action of permanent magnetic eddy current torque and axial force is firstly proposed, and its working principle is firstly elaborated, and the conditions for the establishment of the mechanical seal and the conditions for the switching of the working condition are established, and the equations of the electromagnetic field torque and the axial force equations of this peculiar structure are established, and the correctness of the principle and the design method is finally verified by the calculation of leakage and the analysis of the switching conditions. The following conclusions are drawn.

VII. CONCLUSION

(1) According to the design theory of traditional mechanical seals, the seal establishment and switching conditions under the action of permanent magnetic eddy current torque and axial force are derived, and the corresponding dimensional constraint relations are obtained;

(2) The electromagnetic torque and axial force formulas of the permanent magnet eddy current transmission based on the conductor disk with internal iron ring are established by the method of separated variables, and the analytical results are closer to the results of some meta-analyses in the low-slip region, and the error increases with the increase of rotational speed. It has enough accuracy in the low-slip region to meet the requirements of working conditions.

(3) Through the leakage simulation calculation, the working state of the mechanical seal under cylinder condition and spray condition is revealed, which reflects the effectiveness of the principle of permanent magnetic eddy current mechanical seal switch.

It should be pointed out that this paper only investigates the principle and design theory of the permanent magnet eddy current seal switch, and due to the complexity of its sealing interface work, it is necessary to carry out further detailed tests to study its sealing effect, life and reliability. Optimization of the structural parameters of the permanent magnet coupling structure, which drives the switches, also contributes to the optimization of its performance, but this is not discussed in this paper due to space constraints.

APPENDIX

Detailed boundary conditions:

$$\begin{cases} \dfrac{\partial \mathbf{A}_{1n}}{\partial x} = \dfrac{\partial \mathbf{A}_{2n}}{\partial x}\Big|_{y=\delta_1} \\ \dfrac{1}{\mu_1}\dfrac{\partial \mathbf{A}_{1n}}{\partial y} = \dfrac{1}{\mu_2}\dfrac{\partial \mathbf{A}_{2n}}{\partial y}\Big|_{y=\delta_1} \end{cases} \tag{A1}$$

$$\begin{cases} \dfrac{\partial \mathbf{A}_{2n}}{\partial x} = \dfrac{\partial \mathbf{A}_{3n}}{\partial x}\Big|_{y=\delta_2} \\ \dfrac{1}{\mu_2}\dfrac{\partial \mathbf{A}_{2n}}{\partial y} = \dfrac{1}{\mu_3}\dfrac{\partial \mathbf{A}_{3n}}{\partial y}\Big|_{y=\delta_2} \end{cases} \tag{A2}$$

$$\begin{cases} \dfrac{\partial \mathbf{A}_{3n}}{\partial x} = \dfrac{\partial \mathbf{A}_{4n}}{\partial x}\Big|_{y=\delta_3} \\ \dfrac{1}{\mu_3}\dfrac{\partial \mathbf{A}_{3n}}{\partial y} = \dfrac{1}{\mu_4}\dfrac{\partial \mathbf{A}_{4n}}{\partial y}\Big|_{y=\delta_3} \end{cases} \tag{A3}$$

$$\begin{cases} \dfrac{\partial \mathbf{A}_{4n}}{\partial x} = \dfrac{\partial \mathbf{A}_{5n}}{\partial x}\Big|_{y=\delta_4} \\ \dfrac{1}{\mu_4}\dfrac{\partial \mathbf{A}_{4n}}{\partial y} = \dfrac{1}{\mu_5}\dfrac{\partial \mathbf{A}_{5n}}{\partial y}\Big|_{y=\delta_4} \end{cases} \tag{A4}$$

$$\begin{cases} \dfrac{\partial \mathbf{A}_{5n}}{\partial x} = \dfrac{\partial \mathbf{A}_{6n}}{\partial x}\Big|_{y=\delta_5} \\ \dfrac{1}{\mu_5}\dfrac{\partial \mathbf{A}_{5n}}{\partial y} = \dfrac{1}{\mu_6}\dfrac{\partial \mathbf{A}_{6n}}{\partial y}\Big|_{y=\delta_5} \end{cases} \tag{A5}$$

REFERENCES

[1] L. Faquan, "Research status on internal spraying technology of gateway driving equipment," *Coal Sci. Technol.*, vol. 45, no. 4, pp. 89–92, Apr. 2017.

[2] A. C. Smith, H. Willsamson, N. Benhama, L. Counter, and J. M. Papadopoulos, "Magnetic drive couplings," in *Proc. 9th Int. Conf. Elect.*, 1999, pp. 232–236.

[3] Y. Wenqi and L. Dong, "Design on mine permanent magnet coupler of 40 kW scraper conveyor," *COAL Eng.*, vol. 46, no. 11, pp. 131–133, Nov. 2014, doi: 10.11799/ce201411041.

[4] A. Wallace, "A high efficiency, alignment and vibration tolerant, coupler using high energy-product permanent magnets," in *Proc. 7th Int. Conf. Electr. Mach. Drives*, Durham, U.K., 1995, pp. 232–236, doi: 10.1049/cp:19950869.

[5] Y. Wang and H. Zhang, "Research on the axial force-slip characteristics of permanent magnetic eddy current frictional torque limiter," *Meitan kexue jishu*, vol. 51, no. 4, pp. 198–208, Apr. 2023, doi: 10.13199/j.cnki.cst.2022-1352.

[6] S. Mohammadi, M. Mirsalim, S. Vaez-Zadeh, and H. A. Talebi, "Analytical modeling and analysis of axial-flux interior permanent-magnet couplers," *IEEE Trans. Ind. Electron.*, vol. 61, no. 11, pp. 5940–5947, Nov. 2014, doi: 10.1109/TIE.2014.2311391.

[7] C. Yang, Y. Zhang, T. Zhang, Z. Chen, and L. Kong, "Analysis of axial force of adjustable speed squirrel-cage asynchronous magnetic coupling," *Chin. J. Eng. Des.*, vol. 23, no. 3, pp. 282–287, 2016.

[8] C. Yang, A. Yuan, X. Zhang, Y. Wu, and K. Liu, "Analysis of the adjustable-speed relationship of axial-flux solid asynchronous magnetic coupler," *J. Mech. Transmiss.*, vol. 41, no. 12, pp. 36–42, 2017.

[9] C. Yang and J. Zhu, "Analysis of the torque characteristics of magnetic couplers with magnet spacing arrangement," *Mach. Des. Res.*, vol. 203, no. 1, pp. 180–184, 2023, doi: 10.13952/j.cnki.jofmdr.2023.0037.

[10] Y. Chao-Jun, Y. Ai-Ren, C. Zi-Qing, W. Ying-Zhi, Z. Xiao-Feng, and L. Kang, "Mechanical properties and adjustable-speed characteristics of axial-flux-solid-type asynchronous magnetic couples," *Electric Mach. Control*, vol. 23, no. 5, pp. 110–118,2019, doi: 10.15938/j.emc.2019.05.014.

[11] X. Dai, Q. Liang, J. Cao, Y. Long, J. Mo, and S. Wang, "Analytical modeling of axial-flux permanent magnet eddy current couplings with a slotted conductor topology," *IEEE Trans. Magn.*, vol. 52, no. 2, pp. 1–15, Feb. 2016, doi: 10.1109/TMAG.2015.2493139.

[12] Y. Gao, "Study on magnetic field characteristics and torque performance of slotted disk magnetic coupler," M.Sc thesis, Dept. Mech. Eng., Jiangsu Univ., Nanjing, China, 2022.

[13] W. Teng, W. Zhenghui, W. Yipeng, and G. Wenxiao, "Speed regulation characteristics of variable conductivity-based barrel-type permanent magnet eddy current governor," *IEEE Access*, vol. 11, pp. 30159–30170, 2023, doi: 10.1109/ACCESS.2023.3261561.

[14] E. Mayer, *Mechanical Seals*, 6th ed. Beijing, China: Chemical Industry Press, 1981.

[15] *GB/T 33509–2017 General Specification for Mechanical Seals*, China Nat. Standardization Manag. Committee, Beijing, China, 2017.

[16] W. Nolting, *Theoretical Physics 3 Electrodynamics*, 1st ed. Cham, Switzerland: Springer, 2016, p. 659.

[17] R. L. Russell and K. H. Norsworthy, "Eddy currents and wall losses in screened-rotor induction motors," *Proc. IEE A, Power Eng.*, vol. 105, no. 20, pp. 163–175, Apr. 1958, doi: 10.1049/pi-a.1958.0036.

[18] G. U. Yongquan, "Calculation of the main parameters of the mechanical end seal (3)—Performance parameters (continued) and calculation examples," *Fluid Machinery*, vol. 6, pp. 27–32, Jan. 1996.

WANG TENG was born in Xinjiang, Shanxi, China, in 1964. He received the Ph.D. degree in engineering from Xi'an Jiaotong University, China, in 2006. He is currently with China Coal Technology and Engineering Group (CCTEG) Taiyuan Research Institute Company. His research interests include coal mine machinery design theory, mechanical system dynamics, and control technology.

WU YIPENG received the bachelor's degree in traffic engineering from Tongji University, in 2020. He is currently pursuing the master's degree with the Department of Mechanical Engineering, China Coal Research Institute, Beijing, China. His research interests include permanent magnet eddy current drive, computational fluid dynamics, and their application in coal mine machinery.

SONG TAO was born in Baiyin, Gansu, China, in 1981. He received the master's degree from Xi'an University of Technology, in 2021. He is currently with CCTEG Taiyuan Research Institute Company Ltd., where he is an Associate Researcher.

GUO WENXIAO was born in Wenxi, Shanxi, China, in 1984. He received the Ph.D. degree in engineering from the North University of China, China, in 2021. He is currently with CCTEG Taiyuan Research Institute Company Ltd., where he is an Associate Researcher.